Physics and Imaging in Radiation Oncology 20 (2021) 34–39

Contents lists available at ScienceDirect

Physics and Imaging in Radiation Oncology

journal homepage: www.sciencedirect.com/journal/physics-and-imaging-in-radiation-oncology

Optimisation and validation of an integrated magnetic resonance imaging-only radiotherapy planning solution

Laura M. O'Connor [a,b,*], Kate Skehan [a], Jae H. Choi [c], John Simpson [a,c], Jarad Martin [a,c], Helen Warren-Forward [b], Jason Dowling [d,e], Peter Greer [a,c]

[a] Department of Radiation Oncology, Calvary Mater Hospital, Newcastle, NSW, Australia
[b] School of Health Sciences, University of Newcastle, Newcastle, NSW, Australia
[c] School of Medicine and Public Health, University of Newcastle, Newcastle, NSW, Australia
[d] School of Mathematical and Physical Sciences, University of Newcastle, Newcastle, NSW, Australia
[e] Australian E-Health Research Centre, Commonwealth Scientific and Industrial Research Organisation (CSIRO), Herston, QLD, Australia

ARTICLE INFO

Keywords:
MRI only radiation therapy
Synthetic CT
Radiotherapy
Radiation therapy treatment planning
Prostate cancer
Rectal cancer

ABSTRACT

Background and purpose: Magnetic resonance imaging (MRI)-only treatment planning is gaining in popularity in radiation oncology, with various methods available to generate a synthetic computed tomography (sCT) for this purpose. The aim of this study was to validate a sCT generation software for MRI-only radiotherapy planning of male and female pelvic cancers. The secondary aim of this study was to improve dose agreement by applying a derived relative electron and mass density (RED) curve to the sCT.
Method and materials: Computed tomography (CT) and MRI scans of forty patients with pelvic neoplasms were used in the study. Treatment plans were copied from the CT scan to the sCT scan for dose comparison. Dose difference at reference point, 3D gamma comparison and dose volume histogram analysis was used to validate the dose impact of the sCT. The RED values were optimised to improve dose agreement by using a linear plot.
Results: The average percentage dose difference at isocentre was 1.2% and the mean 3D gamma comparison with a criteria of 1%/1 mm was 84.0% ± 9.7%. The results indicate an inherent systematic difference in the dosimetry of the sCT plans, deriving from the tissue densities. With the adapted RED_{mod} table, the average percentage dose difference was reduced to −0.1% and the mean 3D gamma analysis improved to 92.9% ± 5.7% at 1%/1 mm.
Conclusions: CT generation software is a viable solution for MRI-only radiotherapy planning. The option makes it relatively easy for departments to implement a MRI-only planning workflow for cancers of male and female pelvic anatomy.

1. Introduction

Computed tomography (CT) is currently the primary imaging modality for radiotherapy planning. The CT scan grey level (Hounsfield Units (HU)) values are normalised units of X-ray attenuation, from which relative electron density and mass density can be easily derived via a calibration measurement, allowing for calculation of radiation attenuation in the body [1].

Magnetic Resonance Imaging (MRI) has been increasingly adopted in radiation therapy over recent years, due to the improved tumour and soft tissue visibility [2–7]. Dedicated MRI scanners and MRI-linear accelerator hybrid machines are being introduced into radiation therapy centres, and research into MRI only planning is gaining in popularity [8–10]. In order to accommodate MRI based radiation therapy planning, electron and mass density information has to be derived, a process which has been termed synthetic CT (sCT) creation. Researchers have developed varying methods to define the electron and mass densities of structures derived from MRI scans, to create a sCT from the MRI scan for dose calculation. Two such methods include; tissue class segmentation, in which tissue types are classed into two or more categories, assigning each tissue type an appropriate bulk HU override [11–13], and atlas based segmentation, in which the MRI scan is compared to an atlas of

Abbreviations: DVH, dose volume histogram; HU, Hounsfield Unit; ICRU, International Commission on Radiation Units and Measurements; RED, Relative electron density; sCT, synthetic computed tomography.

* Corresponding author at: Department of Radiation Oncology, Calvary Mater Hospital, Cnr Edith & Platt St, Waratah, Newcastle, NSW 2298, Australia.
E-mail address: Laura.OConnor@calvarymater.org.au (L.M. O'Connor).

https://doi.org/10.1016/j.phro.2021.10.001
Received 31 May 2021; Received in revised form 5 October 2021; Accepted 10 October 2021
Available online 16 October 2021

registered MRI/CT pairs, and an average scan pair or local weighted voting is applied to define the HU on a voxel by voxel basis, to create a sCT [14–16]. Machine learning is also being utilised for MRI planning, and has quickly become a popular method of sCT generation [17,18]. The application of MRI planning has become more widespread, with it being expanded more broadly to be utilised in other radiotherapy based clinical trials [19].

In recent years, sCT generation software products have become available. Such products are based on a tissue class segmentation approach, combined with a multi-atlas-based approach of sCT generation [20]. Some products have been extensively validated in peer reviewed journals, for use in prostate, rectal and gynaecological radiotherapy planning, while other software have had limited validation [13,21–24]. As these products had been released for use in all male and female pelvic radiation therapy planning, there is therefore a need to assess the use of the product for male and female patients with cancers of the prostate and greater pelvis.

This article presents a retrospective study, assessing a sCT generation product for male and female pelvic treatment regions. The aim of the study was to investigate the dose impact and anatomical accuracy of the sCT generation method, and further improved on the dose accuracy of the sCT using a derived modified relative electron density and mass density values for the sCT HU to RED table.

2. Materials and methods

2.1. Patient data collection

Human research ethics committee approval for the study was obtained and forty-one patients receiving radiation treatment to the pelvic region gave informed consent to participate in the trial. Patients were separated into two cohorts for the study; prostate and greater pelvis (gynaecological and colorectal), while one patient was excluded after insufficient coverage of the MRI scan due to user error. Detailed patient demographics are shown in Table 1.

Planning CT scans were acquired on a SOMATOM Confidence CT scanner (Siemens Healthineers; Erlangen, Germany) at 120 kV with 2.0 mm slice thickness and positioning tattoos were placed on the patients to aid in treatment alignment. The prostate cohort were positioned supine, using a knee and ankle immobilisation devices. The greater pelvis cohort were scanned supine, legs flat in a CIVCO vac-lok bag (CIVCO Medical Instruments; Iowa, USA). MRI scans were performed on a MAGNETOM Skyra 3T MRI scanner (Siemens Healthineers; Erlangen, Germany), immediately following the CT scan The MRI scanner was equipped with a Qfix flat couch (Qfix; Pennsylvania USA) and DORADOnova MR 3T external laser bridge (LAP; Luneburg, Germany). Patients were positioned by a radiation therapist and radiographer, using identical ancillary equipment as their CT scan, and aligned using their tattoos and the external laser bridge. An 18 channel body coil was positioned in a Qfix INSIGHT MR Body coil holder over the pelvic region to avoid compression of the external body contour and a 32 channel spine coil was utilised under the flat couch top. All patients were scanned with a full bladder and empty rectum for their CT and MRI scan and minimum scan range included from the top of 3rd lumbar vertebrae, to mid femur.

A standard T1 VIBE DIXON was adapted from the original scanning protocol (see supplementary material A for details), these adaptations made were within the limits outlined in the product terms of use. This sequence was added to the patient's routine MRI scanning protocol and care was taken to ensure the external body contour was included. The MRI was retrospectively post-processed on the SyngoVia (VB30A_HF03) software platform (Siemens Healthineers; Erlangen, Germany) to create the sCT utilising Siemens Healthineers' commercial sCT generation product. The sCT creation process, was a hybrid technique utilising a multi-atlas based registration method to create bony contours (separated into cortical bone and trabeculae bone), a tissue class segmentation method to outline the fat and muscle/visceral tissue, and thresholding to segment air. Each of these five tissue classes were assigned a bulk HU value to create the sCT [20].

Treatment planning was performed using the Eclipse treatment planning system (version 15.6; Varian Medial Systems) and AAA_13623 calculation algorithm. An in-house calibration curve (RED_{CT}) was used for HU to electron and mass density conversion on the conventional CT scan. Thirty-nine patients were planned as 6-MV, 2–3 arc VMAT (Volumetric Modulated Arc Therapy), while one patient in the prostate cohort was planned as 6-MV, 7 field sliding-window IMRT (Intensity Modulated Radiation Therapy) due to radiation oncologist preference.

2.2. Validation

The MRI and paired sCT were imported into the treatment planning system. A HU to RED curve supplied by Siemens Healthineers (RED_{sCT}) was applied to the sCT, values for this curve are outlined in Table 2. The MRI was registered to the planning CT scan using automatic rigid registration, while the sCT was registered to the MRI scan by mutual frame of reference information. The CT based treatment plan and structure set was copied to the sCT and the treatment plans were recalculated with identical monitor unit values and calculation algorithm.

To evaluate dose accuracy, the International Commission on Radiation Units and Measurements (ICRU) reference point for each plan was copied from the CT based plan to the sCT. The dose impact to the planning target volume (PTV) and organs at risk (OAR) was evaluated using relevant dose volume histogram (DVH) parameters for these structures, as per standard guidelines for each treatment site [25–29]. Several DVH parameters were evaluated for each structure, the average dose difference for each structure was a combined average of each of these parameters for each structure. The percentage dose difference was

Table 2
Final values for the supplied and derived modified RED and mass density curves.

Tissue Class	Hounsfield Unit (HU)	Relative Electron Density		Relative Mass Density (g/cm^3)	
		Supplied	Derived	Supplied	Derived
Air	−1000	0.001	0.001	0.001	0.001
Fat	−75	0.950	0.977	0.950	0.991
Muscle/ visceral	0	1.017	1.032	1.022	1.046
Trabeculae	204	1.096	1.125	1.143	1.170
Cortical Bone	1170	1.695	1.451	1.823	1.540

Table 1
Patient Demographics.

	Cohort size	Age range	BMI range (kg/m^2)	Primary treatment site	Staging range	Gender
Prostate Cohort	20	56–80 (mean = 73)	23.3–37.0 (mean = 30.3)	Prostate (n = 20)	T1c-T3b	Male (n = 20)
Greater Pelvis Cohort	20	38–80 (mean = 62)	18.2–36.7 (mean = 26.4)	Rectum (n = 14)	T1N0-T4aN1c	Male (n = 10) Female (n = 4)
				Anal Canal (n = 1)	T2N1	Female (n = 1)
				Cervix (n = 2)	IIB	Female (n = 2)
				Endometrium (n = 3)	IIIA-IIIC	Female (n = 3)

calculated with $(D_{sCT}-D_{CT})/D_{CT}$ * 100%. Statistical significance of the dose difference at ICRU reference point was determined using a paired *t*-test with a significance level of 0.05. Shapiro-Wilk test was used to test for normality of the data to validate the use of the *t*-test. Three-dimensional gamma analysis was used to evaluate the dose impact of the sCT on the treatment plan with reference to the treatment plan on the planning CT scan. This method was performed using an in-house MATLAB code (MATLAB; MathWorks), and included a dose-difference (%) and distance to agreement (mm) of 3%/2 mm, 2%/2 mm, and 1%/1 mm. An erosion of 15 mm of the body perimeter was applied to exclude failures which occur at skin edge due to small unavoidable differences in body contour between data sets. The 3D gamma results were deemed acceptable, if the results for all patients was within American Association of Physics in Medicine (AAPM) TG218 report guidelines of >95% at 3%/2 mm [30].

The anatomical accuracy was assessed for the entire body contour and bony regions on the CT and sCT, using a DICE similarity coefficient DSC = 2[A ∩ B]/A + B and volume comparisons of body and bone contours created for the CT, sCT and MRI data sets for each patient.

2.3. Adaptation of HU to electron density table

Two methods to derive an optimal HU to RED curve were investigated. In the first method a mapping was derived that, when applied to the sCT, gave the same resultant average electron and mass density for the five sCT tissue classes as the in-house CT and RED_{CT} curve ($RED_{sCT,av}$). In the second method a mapping was derived to give average point dose agreement of ~zero to CT and RED_{CT} at isocentre ($RED_{sCT,mod}$).

The entire bone structure was outlined and the fat and muscle/visceral tissue were defined using thresholding on the CT as defined by the fat and muscle/visceral peaks on the tissue density histogram. The volume of cortical bone present on the sCT varied greatly therefore, the cortical bone and trabeculae bone structures were copied from the sCT to the CT scan and restricted to the bony region defined on the CT.

$RED_{sCT,av}$ was created by mapping the tissue class HU values of the sCT to the average electron and mass densities obtained from the corresponding segmented tissue classes from the CT and RED_{CT}. The RED_{ave} was then applied to the sCT, doses recalculated and the percentage dose difference at ICRU reference point to the CT plan was recorded for each patient.

For the second method an RED_{mod} was created, by calculating the optimal relative electron density of each tissue type using Choi et al.'s method of a linear plot, applied to electron density rather than HU [12]. This method relies on the relationship between tissue density and dose difference at the ICRU point. When a higher or lower density is applied to a tissue type, the dose at the reference point is respectively lesser or greater. The percentage dose difference can be plotted against tissue density at two tissue densities, and the equation of a line can be used to derive the ideal tissue density; when the percentage dose difference between CT and sCT equals zero, for each tissue type separately. Optimal values were investigated for each tissue type to create the $RED_{sCT,mod}$ curve, which was then applied to the sCT and doses were re-calculated on both the CT and sCT using AcurosXB_15605 dose to medium calculation algorithm.

3. Results

The 3D gamma results for the sCT with the supplied RED_{sCT} applied are outlined in Table 3. The results were deemed acceptable, as the gamma pass rate for all patients were within AAPM TG218 report guidelines, with a 99.6% ± 1.0 (mean ± 1 SD) pass rate at a criteria of 3%/2 mm for all patients. At a criteria of 1%/1 mm, the pass rate was 84.0% ± 9.7 for all patients, with a higher pass rate in the prostate subgroup (88.6% ± 5.3) than the greater pelvis subgroup (79.5% ± 11.0).

The percentage dose difference was statistically significant ($t = 8.14$, $p < 0.005$) between the treatment plan on the CT and the sCT (RED_{sCT}) at the ICRU reference point for all patients at 1.2% ± 0.9% (range 0.8% − 3.9%); 1.3% ± 0.6% for prostate subgroup and 1.1% ± 1.1% for greater pelvis subgroup. The DVH percentage dose difference for all parameters combined was 1.0% ± 1.4% for all patients, 0.9% ± 1.9% for prostate subgroup, and 1.1% ± 0.6% for greater pelvis subgroup (Fig. 2). The greatest discrepancy in DVH results was for the bladder in the prostate subgroup (0.8% ±5.1%). The greater variation was due to outliers, however these corresponded to very low dose values, the average absolute dose differences for these was less than 1.0 Gy.

On average, the sCT tissue volume was greater than the MRI (0.5% ± 1.5%) and CT (0.1% ± 1.2%) tissue volume. The sCT bone volume was greater than the MRI volume (0.1% ± 3.8%) and lesser than the CT volume (20.2% ± 6.9%). The Dice similarity coefficient for the MRI and sCT bone was 0.95 ± 0.04, and for the MRI to sCT tissue was 0.99 ± 0.0.

When a uniform electron density equivalent to water, was applied to the body contour for both the CT and sCT, and the treatment plans on each was recalculated. The differences in body contour was found to have the greatest dose impact in the 1%/1 mm criteria of the 3D gamma dose comparison pass rate, for the greater pelvis cohort (93.5%) than the prostate cohort (99.2%). Indicating that body variations, away from the ICRU reference point, had a greater effect on the greater pelvis cohort than the prostate cohort.

The resulting mean difference in relative electron density was greater on the CT scan for fat (+0.002), muscle/visceral (+0.015) and trabeculae bone (+0.029), while cortical bone was lesser (−0.244).

3.1. Adaptation of HU to electron density table

When the optimal RED values were calculated, cortical bone and trabeculae bone gave the greatest difference between the prostate and greater pelvis cohorts, therefore the bone tissue types were fixed at their average values for the final $RED_{sCT,mod}$ model. Fat and muscle gave a similar results between the prostate and the greater pelvis cohort. The optimal value for fat, derived from the linear plot (Fig. 1), was within the range of values derived from the CT, for this tissue type in the cohort. The optimal value for muscle did not fall within the range of values. Therefore, the optimal value for fat was used, and the average value for muscle used in the final $RED_{sCT,mod}$ model. The final relative electron density values were used to derive the corresponding mass density

Table 3
3D Gamma analysis results for all patients (n = 40), prostate cohort (n = 20) and greater pelvis cohort (n = 20) for plans on sCT with Siemens Healthineers' RED_{sCT} applied.

	3%/2 mm		2%/2 mm		1%/1 mm	
	Pass Rate (%)	Av Gamma	Pass Rate (%)	Av Gamma	Pass Rate (%)	Av Gamma
All Patients	99.6 ± 1.0	0.18 ± 0.07	98.5 ± 2.6	0.27 ± 0.09	84.0 ± 9.7	0.53 ± 0.17
range	100.0–96.1	0.03–0.38	100.0–86.8	0.05–0.54	100–52.0	0.10–1.07
Prostate	100.0 ± 0.1	0.15± 0.04	99.7 ± 0.4	0.22 ± 0.06	88.6 ± 5.3	0.44 ± 0.11
range	100.0–99.7	0.03–0.21	100.0–98.3	0.05–0.30	100.0–79.6	0.10–0.59
Greater Pelvis	99.1 ± 1.4	0.22 ± 0.07	97.3 ± 3.3	0.31 ± 0.09	79.5 ± 11.0	0.63 ± 0.18
Range	100.0–96.1	0.15–0.38	99.6–86.8	0.21–0.54	91.1–52.0	0.43–1.07

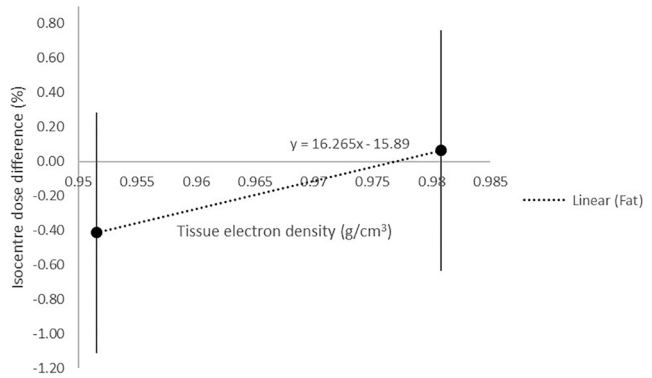

Fig. 1. Linear relationship between the mean isocentre dose differences for two fat tissue electron density values ±1 SD. The x-intercept represents the optimal electron density used for fat.

values from the RED_{CT} curve, and both mapped to the HU values of the sCT to create the final $RED_{sCT,mod}$, these values are outlined in Table 2.

With the RED_{ave} applied, the percentage dose difference at ICRU reference point was 0.4% ± 0.7. With the $RED_{sCT,mod}$ (Table 2) curve applied to the sCT the percentage dose difference at the ICRU reference point improved to −0.1% ± 0.8 (range = −1.6–2.0), with no statistically significant difference between the CT and sCT values (t = −1.2, p = 0.2) for all patients. The DVH results for the all parameters combined improved to −0.1% ± 1.4% for all patients, −0.2% ± 1.8% for the prostate subgroup and −0.1% ± 0.9% for the greater pelvis subgroup (Fig. 2). The gamma results for all patients were within the AAPM TG218 report guidelines with a pass rate of 99.8% ± 0.5 at a criteria of 3%/2mm for all patients. The 3D gamma analysis outlined in Table 4, showed improved agreement, most notably at a criteria of 1%/1mm, of which the pass rate was 92.9% ± 5.7 for all patients, with a higher pass rate for the prostate subgroup (96.0% ± 2.0) than the greater pelvis subgroup (89.8% ± 6.5). The $RED_{sCT,mod}$ was derived using AAA_13623 algorithm and tested on AcurosXB_15605 dose to medium calculation algorithm to test if the derived values of electron density and mass density are applicable to algorithms which calculate based separately on

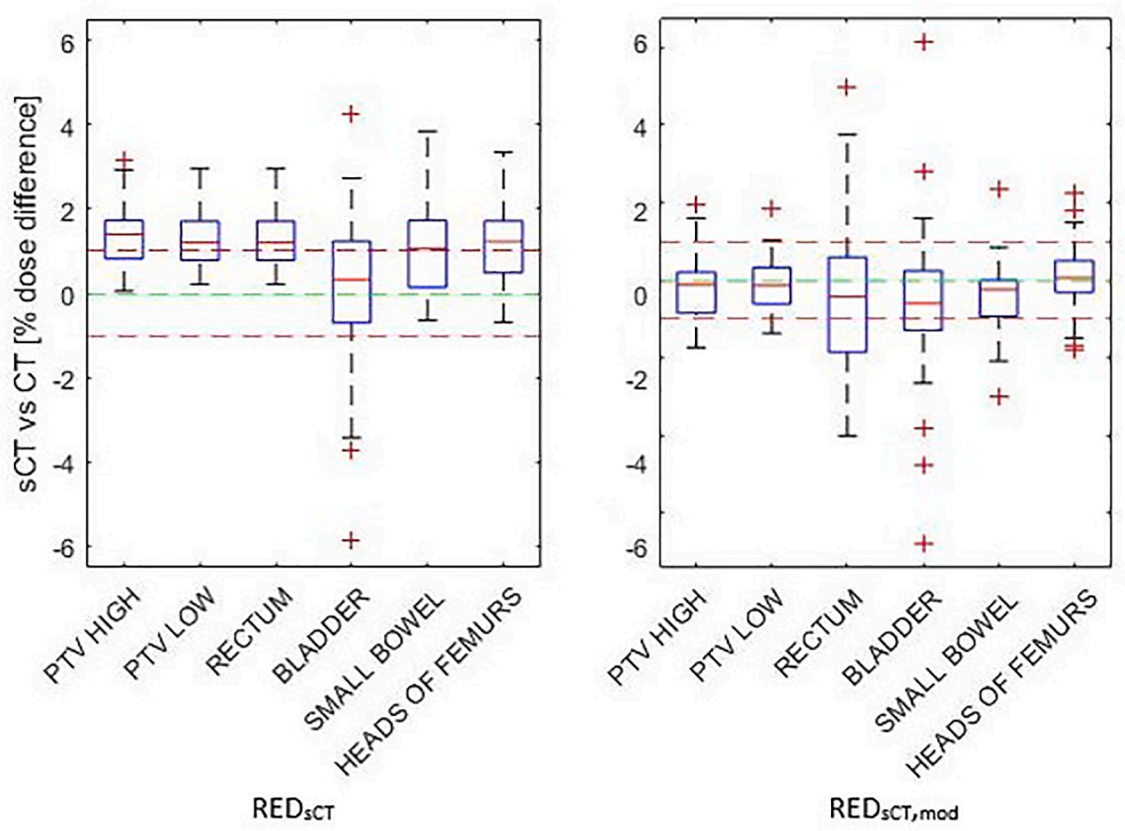

Fig. 2. DVH results by structure for REDsCT and REDsCT,mod applied to sCT.

Table 4
Gamma analysis results for all patients (n = 40), prostate cohort (n = 20) and greater pelvis cohort (n = 20) for plans on sCT with a derived curve $RED_{sCT,mod}$ applied.

	3%/2 mm		2%/2 mm		1%/1 mm	
	Pass Rate (%)	Av Gamma	Pass Rate (%)	Av Gamma	Pass Rate (%)	Av Gamma
All Patients	99.8 ± 0.5	0.14 ± 0.04	99.6 ± 0.9	0.2 ± 0.1	92.9 ± 5.7	0.4 ± 0.1
range	100.0–97.5	0.08–0.27	100.0–95.3	0.12–0.37	98.3–71.1	0.24–0.77
Prostate	100.0 ± 0.1	0.12 ± 0.02	99.9 ± 0.1	0.16 ± 0.03	96.0 ± 2.0	0.30 ± 0.08
range	100.0–99.8	0.08–0.16	100.0–99.5	0.12–0.25	98.3–91.1	0.24–0.41
Greater Pelvis	99.6 ± 0.7	0.16 ± 0.04	99.2 ± 1.1	0.22 ± 0.05	89.8 ± 6.5	0.44 ± 0.11
range	100.0–97.5	0.11–0.27	99.9–95.3	0.17–0.37	94.9–71.1	0.33–0.77

electron density and mass density values.

4. Discussion

The results of the analysis of a commercial sCT product, presented in this article, appeared to have a systematic difference resulting in average percentage dose difference between the CT and sCT of 1.2%. The results aligned with difference in the average tissue values for the tissue classes on the sCT compared to the CT. As the output of HU values cannot be controlled by the user in commercial sCT products, this study took a novel approach to applying Choi et al.'s linear plot to derive a suitable $RED_{sCT,mod}$ table to give optimal dose results [12]. The application of the derived modified density curve reduced the average percentage dose difference at ICRU reference point, the DVH parameters and the 3D gamma comparison between the plan on the CT and sCT. This indicated that the derived density curve method was successful in improving the dose results for the sCT data set.

The results presented for MRI only radiotherapy planning in this study can be compared to similar studies performed on other sCT generation software, for patients with prostate, rectal and gynaecological cancers [22]. The mean dose difference at reference point, DVH parameters and 3D gamma comparison was slightly lower for Tyagi et al.'s study than this study, with the supplied density curve, however with the derived curve applied to the sCT, the results are very similar [22]. The results presented in this paper also compare favourably to other sCT methods such as a manual tissue class segmentation method and a multi-atlas based with patch based local weighted voting method applied to prostate cancer treatments, where the multi-atlas based method gave a slightly higher agreement in reference point dose difference and gamma pass rate [15].

The availability of sCT software makes MRI planning more accessible and viable for clinical departments, resulting in a more widespread application and utilisation of MRI only planning. These sCT generation methods have the advantage of the ability to apply the model on male and female pelvic anatomy, the speed of sCT generation, and coverage of the sCT model; opening the scope to treat more patients with a MRI only planning workflow. However, sCT software products are not without their potential sources of uncertainty. It is recommended by the authors that departments utilise similar dosimetry validation methods presented in this study, for sCT software commissioning. An approach has been demonstrated in this study for deriving a density curve that yielded more accurate dose results, however these results apply to our departmental density curves, if departments are looking at adopting this adaptation, it is advised to perform similar validation.

This study has shown that a sCT generation software is a viable solution for MRI only radiotherapy planning for male and female patients with pelvic cancer. Although a systematic source of dose difference was identified, the gamma dose agreement was within the AAPM guidelines of >95% pass rate with a criteria of 3%/2 mm. Additionally the dose difference is still relatively low and most likely within department tolerances for treatment planning.

5. Disclosures

We would like to acknowledge Siemens Healthineers for providing the sCT software for the SyngoVia platform. Ethics approval was granted through Hunter New England ethics committee.

6. Data availability

Ethics approval for this study does not allow for sharing of individual patient scans. Other study data, which does not include patient data sets, are available from the corresponding author on reasonable request.

Declaration of Competing Interest

The authors declare that they have no known competing financial interests or personal relationships that could have appeared to influence the work reported in this paper.

References

[1] Khan FM, Gibbons JP. The physics of radiation therapy. 4th ed. Lippincott Williams & Wilkins; 2009.
[2] Metcalfe P, Liney GP, Holloway L, Walker A, Barton M, Delaney GP, et al. The potential for an enhanced role for MRI in radiation-therapy treatment planning. Technol Cancer Res Treat 2013;12(5):429–46. https://doi.org/10.7785/tcrt.2012.500342.
[3] Sabater S, Pastor-Juan MDR, Berenguer R, Andres I, Sevillano M, Lozano-Setien E, et al. Analysing the integration of MR images acquired in a non-radiotherapy treatment position into the radiotherapy workflow using deformable and rigid registration. Radiother Oncol 2016;119(1):179–84. https://doi.org/10.1016/j.radonc.2016.02.032.
[4] Ng SP, Cardenas CE, Elhalawani H, Pollard C, Elgohari B, Fang P, et al. Comparison of tumor delineation using dual energy computed tomography versus magnetic resonance imaging in head and neck cancer re-irradiation cases. Phys Imaging Radiat Oncol 2020;14:1–5. https://doi.org/10.1016/j.phro.2020.04.001.
[5] Olsson LE, Johansson M, Zackrisson B, Blomqvist LK. Basic concepts and applications of functional magnetic resonance imaging for radiotherapy of prostate cancer. Phys Imaging Radiat Oncol 2019;9:50–7. https://doi.org/10.1016/j.phro.2019.02.001.
[6] Zamboglou C, Eiber M, Fassbender TR, Eder M, Kirste S, Bock M, et al. Multimodal imaging for radiation therapy planning in patients with primary prostate cancer. Phys Imaging Radiat Oncol 2018;8:8–16. https://doi.org/10.1016/j.phro.2018.10.001.
[7] Kuisma A, Ranta I, Keyriläinen J, Suilamo S, Wright P, Pesola M, et al. Validation of automated magnetic resonance image segmentation for radiation therapy planning in prostate cancer. Phys Imaging Radiat Oncol 2020;13:14–20. https://doi.org/10.1016/j.phro.2020.02.004.
[8] Lagendijk JJW, Raaymakers BW, Raaijmakers AJE, Overweg J, Brown KJ, Kerkhof EM, et al. MRI/linac integration. Radiother Oncol 2008;86:25–9. https://doi.org/10.1016/j.radonc.2007.10.034.
[9] Palmér E, Karlsson A, Nordström F, Petruson K, Siversson C, Ljungberg M, et al. Synthetic computed tomography data allows for accurate absorbed dose calculations in a magnetic resonance imaging only workflow for head and neck radiotherapy. Phys Imaging Radiat Oncol 2021;17:36–42. https://doi.org/10.1016/j.phro.2020.12.007.
[10] Maspero M, Tyyger MD, Tijssen RHN, Sevinck PR, Intven MPW, van den Berg CAT. Feasibility of magnetic resonance imaging-only rectum radiotherapy with a commercial synthetic computed tomography generation solution. Phys Imaging Radiat Oncol 2018;7:58–64. https://doi.org/10.1016/j.phro.2018.09.002.
[11] Karotki A, Mah K, Meijer G, Meltsner M. Comparison of bulk electron density and voxel-based electron density treatment planning. J Appl Clin Med Phys 2011;12(4):97–104. https://doi.org/10.1120/jacmp.v12i4.3522.
[12] Choi JH, Lee D, O'Connor L, Chalup S, Welsh JS, Dowling J, et al. Bulk anatomical density based dose calculation for patient-specific quality assurance of MRI-only prostate radiotherapy. Front Oncol 2019;9:997. https://doi.org/10.3389/fonc.2019.00997.
[13] Kemppainen R, Suilamo S, Tuokkola T, Lindholm P, Deppe MH, Keyrilainen. Magnetic resonance-only simulation and dose calculation in external beam radiation therapy: a feasibility study for pelvic cancers. Acta Oncol 2017;56(6):792–8. https://doi.org/10.1080/0284186X.2017.1293290.
[14] Dowling JA, Lambert J, Parker J, Salvado O, Fripp J, Capp A, et al. An atlas-based electron density mapping method for magnetic resonance imaging (MRI)-alone treatment planning and adaptive MRI-based prostate radiation therapy. Int J Radiat Oncol Biol Phys 2012;83(1):e5–11. https://doi.org/10.1016/j.ijrobp.2011.11.056.
[15] Dowling JA, Sun J, Pichler P, Rivest-Hénault D, Ghose S, Richardson H, et al. Automatic substitute computed tomography generation and contouring for magnetic resonance imaging (MRI)-alone external beam radiation therapy from standard MRI sequences. Int J Radiat Oncol Biol Phys 2015;93(5):1144–53. https://doi.org/10.1016/j.ijrobp.2015.08.045.
[16] Arabi H, Koutsouvelis N, Rouzaud M, Miralbell R, Zaidi H. Atlas-guided generation of pseudo-CT images for MRI-only and hybrid PET-MRI-guided radiotherapy treatment planning. Phys Med Biol 2016;61(17):6531–52. https://doi.org/10.1088/0031-9155/61/17/6531.
[17] Maspero M, Savenije MHF, Dinkla AM, Seevinck PR, Intven MPW, Jurgenliemk-Schulz IM, et al. Dose evaluation of fast synthetic-CT generation using a generative adversarial network for general pelvis MR-only radiotherapy. Phys Med Biol 2018;63(18):185001. https://doi.org/10.1088/1361-6560/aada6d.
[18] Han X. MR-based synthetic CT generation using a deep convolutional neural network method. Med Phys 2017;44(4):1408–19. https://doi.org/10.1002/mp.12155.
[19] Martin J, Keall P, Siva S, Greer P, Christie D, Moore K, et al. TROG 18.01 phase III randomised clinical trial of the Novel Integration of New prostate radiation schedules with adJuvant Androgen deprivation: NINJA study protocol. BMJ Open 2019;9:e030731. https://doi.org/10.1136/bmjopen-2019-030731.

[20] Siemens Healthcare GmbH. MR-only RT planning for brain and pelvis with Synthetic CT White paper. https://www.siemens-healthineers.com/magnetic-resonance-imaging/clinical-specialities/synthetic-ct; 2019 [accessed 23 July 2021].
[21] Köhler M, Vaara T, Van Grootel M, Hoogeveen R, Kemppainen R, Renisch S. MR-only simulation for radiotherapy planning. White paper: Philips MRCAT for prostate dose calculations using only MRI data. Koninklijke Philips N.V.;2015.
[22] Tyagi N, Fontenla S, Zhang J, Cloutier M, Kadbi M, Mechalakos J, et al. Dosimetric and workflow evaluation of first commercial synthetic CT software for clinical use in pelvis. Phys Med Biol 2017;62(8):2961-2975. https://doi.org/ 10.1088/1361-6560/aa5452.
[23] Thorwarth D, Warschburger C, Monnich D, Grosse U, Kundel M, Nikolaou, et al. Synthetic CT generation for the pelvic region based on dixon-MR sequences: workflow, dosimetric quality and daily patient positioning. In: Hellwich A, editor. Siemens MAGNETOM Flash. Erlangen: Siemens Healthcare GmbH; 2019, p. 23-27.
[24] Gonzalez-Moya A, Dufreneix S, Ouyessad N, Guillerminet C, Autret D. Evaluation of a commercial synthetic computed tomography generation solution for magnetic resonance imaging-only radiotherapy. J Appl Clin Medical Phys 2021;22(6):191–7. https://doi.org/10.1002/acm2.13236.
[25] Cancer Institute NSW. Clinical Resource: Colorectal rectum neoadjuvant EBRT chemoradiation pre-operative long-course V.6, https://www.eviq.org.au/radiation-oncology/colorectal/1863-rectal-neoadjuvant-ebrt-chemoradiation-pre-op; 2021 [accessed 23 July 2021].
[26] Cancer Institute NSW. Clinical Resource: Gynaecological endometrium adjuvant EBRT V.6. https://www.eviq.org.au/radiation-oncology/gynaecological/233-gynaecological-endometrium-adjuvant-ebrt; 2019 [accessed 23 July 2021].
[27] Cancer Institute NSW. Clinical Resource: Anal definitive EBRT chemoradiation V.5. https://www.eviq.org.au/radiation-oncology/colorectal/1860-anal-definitive-ebrt-chemoradiation; 2021 [accessed 23 July 2021].
[28] Cancer Institute NSW. Clinical Resource: Prostate adenocarcinoma definitive EBRT hypofractionation V.3. https://www.eviq.org.au/radiation-oncology/urogenital/prostate/3370-prostate-adenocarcinoma-definitive-ebrt-hypof; 2019 [accessed 23 July 2021].
[29] Cancer Institute NSW. Clinical Resource: Gynaecological Cervix adjuvant EBRT V.3. https://www.eviq.org.au/radiation-oncology/gynaecological/3026-gynaecological-cervix-adjuvant-ebrt-chemoradi; 2019 [accessed 23 July 2021].
[30] Miften M, Olch A, Mihailidis D, Moran J, Pawlicki T, Molineu A, et al. Tolerance limits and methodologies for IMRT measurement-based verification QA: Recommendations of AAPM Task Group No. 218. Med Phys 2018;45:4:e53-e83. https://doi.org/10.1002/mp.12810.